Nanoscale

ROYAL SOCIETY OF CHEMISTRY

COMMUNICATION

View Article Online
View Journal

Open Access Article. Published on 11 February 2026. Downloaded on 2/26/2026 3:44:54 AM.
This article is licensed under a Creative Commons Attribution 3.0 Unported Licence.

Check for updates

Cite this: DOI: 10.1039/d5nr04690d

Received 5th November 2025,
Accepted 10th February 2026

DOI: 10.1039/d5nr04690d

rsc.li/nanoscale

Coacervate microenvironments modulate fluorescent dye behaviour and Förster energy transfer dynamics

Mohit Kumar,† Minea Kapidžić† and Shikha Dhiman *

Coacervates offer dynamic environments for molecular organization. Using complex coacervates of poly-L-lysine and anionic fluorophores, we show that the coacervate microenvironment modulates dye photophysical properties through competing effects: fluorescence enhancement *via* local enrichment and aggregation-induced quenching at higher loading, while enabling energy transfer. These insights establish coacervates as versatile templates for designing adaptive nanoscale photonic and energy-transfer materials.

Department of Chemistry, Johannes Gutenberg University Mainz, Duesbergweg 10-14, Mainz, 55122, Germany. E-mail: Shikha.dhiman@uni-mainz.de; https://www.dhimanlab.com

†These authors contributed equally.

Shikha Dhiman

Shikha Dhiman is Professor of Physical Chemistry of Supramolecular Systems at the Department of Chemistry, Johannes Gutenberg University Mainz and Junior Faculty at the Max Planck Graduate Center, Mainz. Her research lies at the interface of supramolecular chemistry and biological systems, with a focus on understanding molecular structure–dynamics–function relationships and developing life-like systems inspired by nature. She earned her PhD from JNCASR, Bangalore, followed by postdoctoral research at Eindhoven University of Technology. She has received several distinctions, including the Thieme Chemistry Award 2024 and Marie Skłodowska-Curie Fellowship 2021.

Introduction

Coacervates are compartments formed through liquid–liquid phase separation of (macro)molecules.[1] Their fluid yet compartmentalized structure provides a unique environment where nanoscale interactions can be modulated by electrostatics, hydration, and crowding, features that bridge biological phase separation with materials design. Initially studied as models for membraneless organelles and drug delivery vehicles, they are now emerging as versatile soft-material platforms capable of dynamic molecular organization and responsive functionality.[2–4]

Beyond biological relevance, coacervates have gained increasing attention as adaptive building blocks for responsive and reconfigurable systems.[1,5–7] Their phase behaviour can be precisely tuned by environmental parameters such as pH, ionic strength, and temperature, enabling self-healing, stimuli-responsiveness, and controlled adhesion.[8–15] Incorporation of inorganic components—including metal ions, metal–organic frameworks, and perovskites—has yielded hybrid coacervates with enhanced mechanical, ionic, and optical properties.[16–18] These hybrid systems have enabled diverse applications such as catalytic interfaces, soft robotics, and adaptive coatings.[19]

A hallmark feature of coacervates is their exceptionally high loading capacity, allowing dense encapsulation of small molecules, dyes, and enzymes.[20,21] This has motivated their exploration as microreactors and templating media, where confinement promotes selective reactivity and controlled nanostructure formation.[11,22,23] Unlike rigid hosts such as hydrogels or mesoporous silica, coacervates present a dynamic and ionically heterogeneous microenvironment.[24,25] Therefore, beyond catalysis, such confinement can profoundly alter optical and photophysical properties. These characteristics make coacervates compelling templates for designing responsive materials, energy transfer systems, and light-harvesting assemblies where molecular proximity, polarity gradients, and dynamic interactions govern fluorescence behaviour and exciton dynamics.[26–28]

Open Access Article. Published on 11 February 2026. Downloaded on 2/26/2026 3:44:54 AM.
This article is licensed under a Creative Commons Attribution 3.0 Unported Licence.

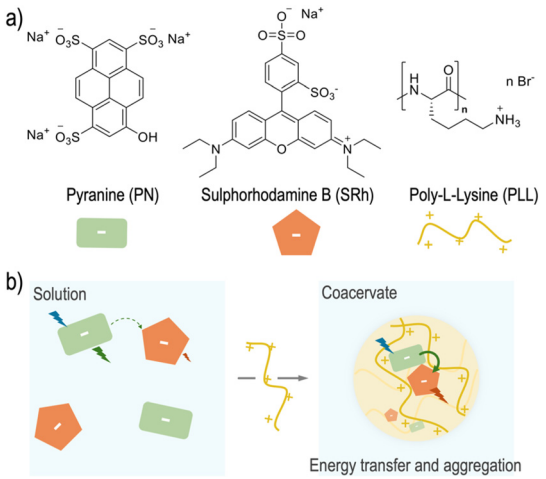

Scheme 1 (a) Chemical structure of PN, SRh, and PLL. (b) Schematic illustration of the energy transfer process within PN–PLL coacervates. In solution, PN (donor) and SRh (acceptor) show limited interaction. Upon coacervation with PLL, molecular confinement and close spatial organization promote efficient energy transfer between PN and SRh.

Herein, we investigate how the coacervate microenvironment modulates the fluorescence and energy-transfer behaviour of encapsulated dyes. Using poly-L-lysine (PLL) as a model cationic scaffold and anionic fluorescent guests 8-hydroxypyrene-1,3,6-trisulfonate (PN) and sulforhodamine B (SRh) as probes, we examine how coacervation influences the emission intensity, aggregation, and FRET efficiency.[29] We show that coacervates exert a dual effect: fluorescence enhancement *via* local enrichment and aggregation-induced quenching at higher loading. Their charged networks can co-localize donor and acceptor species to facilitate efficient energy transfer (Scheme 1). These findings provide mechanistic insight into how electrostatic confinement and molecular crowding govern optical behaviour within soft, dynamic coacervate compartments, establishing a foundation for designing nanoscale photonic and energy-transfer materials based on coacervate architectures.

Results and discussion

To elucidate how fluorescent dyes behave within coacervate microenvironments, we employed PLL, a cationic polypeptide that readily undergoes complex coacervation with multivalent anionic species. As a multivalent fluorescent anion, we used PN that carries three sulfonate groups and has a dual function: serves as a counterion for coacervate formation and as the donor. The anionic guest, SRh, acts as the acceptor; their spectral overlap—where SRh absorption overlaps sufficiently with PN emission—makes them an efficient Förster Resonance Energy Transfer (FRET) pair (Scheme 1).

To prepare the coacervates, PN was titrated with increasing concentrations of PLL. A pronounced increase in turbidity was observed above a PN concentration of 3 mM, while negligible turbidity changes occurred at lower concentrations (0.5 and 1 mM) (Fig. 1a and Fig. S1). The corresponding fluorescence titration measurements revealed a progressive quenching of

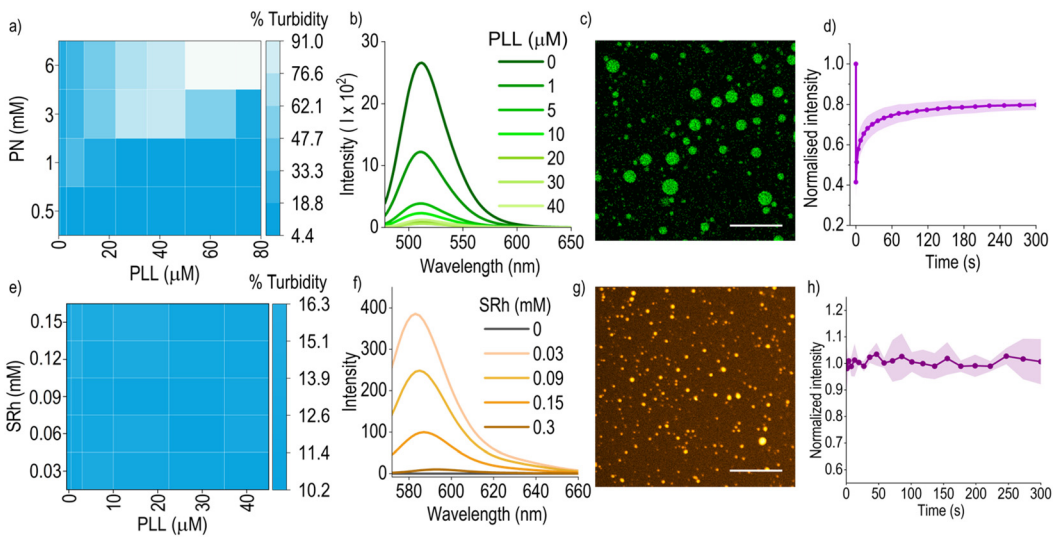

Fig. 1 (a) Turbidity heat map as a function of PN and PLL concentrations showing coacervate formation above 3 mM PN. (b) Fluorescence spectra of PN (3 mM) with increasing PLL concentration, indicating quenching of PN emission (λ_{ex} = 458 nm). (c) CLSM images of PN–PLL coacervates (3 mM PN, 40 μM PLL) showing retained PN fluorescence within the coacervate phase. (d) FRAP kinetics of PN–PLL coacervates with Cy5 dye (0.02 mM) showing the liquid nature of coacervates. (e) Turbidity heat map as a function of SRh and PLL concentrations showing no coacervation with increasing PLL concentration. (f) Fluorescence spectra of SRh in PLL–ATP coacervates (5 mM ATP, 15 μM PLL) showing quenching of SRh emission with increasing SRh concentration (0.03–3 mM, λ_{ex} = 561 nm). (g) CLSM images of PLL–ATP coacervates (5 mM ATP, 15 μM PLL) containing SRh (0.06 mM) showing retained fluorescence. (h) FRAP kinetics of PLL-ATP coacervates (5 mM ATP, 15 μM PLL, 0.02 mM Cy5) showing its liquid nature. Error bars represent average and standard deviation of 3 independent experiments. Scale bar = 20 μm.

 This journal is © The Royal Society of Chemistry 2026

Open Access Article. Published on 11 February 2026. Downloaded on 2/26/2026 3:44:54 AM.
This article is licensed under a Creative Commons Attribution 3.0 Unported Licence.

PN emission, attributable to an increase in local PN concentration within the coacervate droplets, leading to aggregation-induced quenching (Fig. 1b).[30–32] Confocal laser scanning microscopy (CLSM) confirmed the formation of spherical, micron-sized, fluorescent coacervates (Fig. 1c, S2 and Table S1). Due to pronounced scattering within the coacervate phase, acquisition of a reliable absorption spectrum is not feasible. Therefore, we instead analysed the excitation spectrum of PN in the coacervate phase, which exhibited a pronounced red shift and a change in spectral shape compared to the solution state in the absence of PLL, providing evidence for aggregation-induced quenching (Fig. S3). Interestingly, PN emission was only partially quenched, indicating that despite local aggregation, a fraction of the fluorophores remained emissive (Fig. 1c). Notably, when comparing $I_{coacervates}/I_{dilute}$ at 3 mM and 6 mM PN, a decrease in intensity ratio was observed, further supporting aggregation-induced quenching (Fig. S4). Such partial quenching underscores the complexity of dye behaviour in coacervate media, where local crowding and electrostatic effects coexist. Variations in fluorescence intensity directly influence the determination of partition coefficients (K_p) from CLSM measurements, which often assume invariant dye emission within the coacervate phase.

The coacervates exhibited predominantly liquid-like behaviour, as demonstrated by fluorescence recovery after photobleaching (FRAP), where rapid fluorescence recovery was observed (Fig. 1d and S5). This confirms that coacervates retain substantial molecular mobility, while still imposing crowding that can enhance the local dye concentration and promote aggregation.

On the other hand, FRAP experiments with coacervates formed at higher PN concentration (6 mM PN, 40 μM PLL) show recovery lower by 10% compared to coacervates formed at lower PN concentration, indicating a denser internal environment and thus reduced mobility (Fig. S6 and S7). The retained residual brightness of PN ensures its continued suitability as a FRET donor. For all subsequent experiments, a PN (3 mM) and PLL (40 μM) were employed, where PN remains fluorescent within the coacervate phase. Analogous titrations of SRh with increasing PLL concentrations revealed no significant turbidity increase, suggesting the absence of coacervation under these conditions and thus confirming that SRh functions only as a guest, without participating in coacervate formation (Fig. 1e).[33] To assess the influence of the coacervate microenvironment on SRh emission, SRh was instead encapsulated within pre-formed ATP–PLL coacervates. Increasing SRh concentration led to a decrease in its fluorescence intensity, indicating aggregation-induced quenching similar to that observed for PN (Fig. 1f). In the solution state, the SRh emission intensity was 22-fold higher than that in the coacervate phase (Fig. S8). CLSM imaging confirmed partial fluorescence retention within SRh-containing coacervates, consistent with incomplete quenching (Fig. 1g). PLL–ATP coacervates also exhibited liquid-like behaviour, as demonstrated by FRAP; however, fluorescence recovery occurred on a timescale faster than the temporal resolution of the CLSM setup, preventing reliable capture of a well-defined bleaching spot (Fig. 1h and S9). For both systems, the K_p values for PN and SRh were determined to be 40.7 ± 4.9 and 42.7 ± 7 for PN–PLL (3 mM PN, 0.06 mM SRh) and 2.6 ± 0.1 for PLL–ATP–SRh (0.06 mM SRh). It should be noted that partition coefficients derived from CLSM intensities represent semi-quantitative estimates, as local fluorescence modulation within the coacervate phase may influence absolute values.

Given the strong spectral overlap between PN emission and SRh absorption, these dyes constitute an efficient FRET donor–acceptor pair (Fig. S10). Fluorescence and CLSM analysis confirmed co-localization of both dyes within the dense coacervate phase (Fig. S11). Quantitative CLSM analysis demonstrated a high K_p for both PN and SRh, confirming their preferential enrichment within coacervates. Incremental increase in the concentration of encapsulated SRh (0.03 to 0.15 mM) within PN–PLL coacervates caused no significant change in turbidity, indicating that SRh incorporation did not perturb coacervate stability (Fig. S12). The average zeta potential (ζ) of PN-PLL coacervates was measured to be $\zeta < 10$ mV, which implies a near-neutral charge at the coacervate–water interface (Table S2). Encapsulation of SRh did not significantly affect ζ, further confirming that the coacervate microenvironment was not disturbed by the presence of SRh. However, PN emission progressively decreased, suggesting energy transfer from PN to SRh (Fig. S13). Correspondingly, SRh emission increased modestly and exhibited a gradual red shift with increasing SRh concentration, consistent with dye aggregation within the crowded coacervate environment (Fig. 2a and S14). Direct absorption measurements within the coacervate phase could not be reliably obtained due to strong light scattering; therefore, aggregation-related interpretations are based on qualitative emission trends rather than absorption band analysis. The critical aggregation concentration was determined to be approximately 0.06 mM SRh loading in PN–PLL coacervates.

These observations are consistent with a significant contribution from Förster Resonance Energy Transfer (FRET) to PN fluorescence quenching within the coacervate phase, rather than being dominated by reabsorption or collisional quenching. Donor emission is significantly quenched in the coacervate state, whereas only slight quenching is observed in bulk solution, demonstrating that energy transfer requires close spatial confinement (Fig. 2b, S15 and 16). The charged and crowded matrix of PLL coacervates confines donor and acceptor molecules within nanometer proximity, providing the conditions necessary for efficient FRET. Two-channel CLSM imaging further corroborated these findings, revealing a decrease in PN fluorescence and a concomitant increase in SRh emission as the SRh concentration increased, confirming FRET occurrence within the coacervate phase (Fig. 2c, d and S17). At 0.03 mM and 0.06 mM SRh loading—conditions minimizing aggregation—the calculated FRET efficiencies (ϕ_{ET}) were 34.4 ± 0.2% and 50.8 ± 5.2%, respectively (Fig. 2e). Notably, SRh emission in solution exhibited no red shift, confirming that in the absence of PLL, electrostatic repulsion

Open Access Article. Published on 11 February 2026. Downloaded on 2/26/2026 3:44:54 AM.
This article is licensed under a Creative Commons Attribution 3.0 Unported Licence.

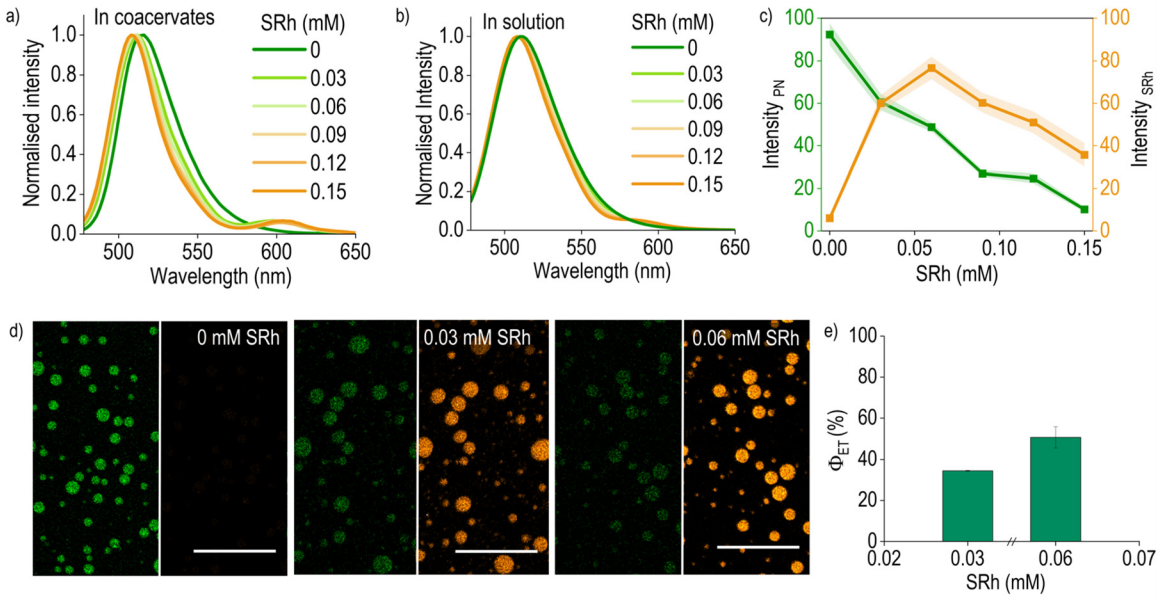

Fig. 2 (a) Normalised fluorescence spectra of PLL–PN coacervates with increasing concentrations of SRh (0–0.15 mM), showing quenching of PN emission, λ_{ex} = 458 nm. (b) Normalised fluorescence spectra of PN with increasing concentrations of SRh (0–0.15 mM) in solution, λ_{ex} = 458 nm. (c) Plot of average fluorescence intensity of PN and SRh in PLL–PN coacervates extracted from CLSM images at different SRh concentrations (0–0.15 mM) λ_{ex} = 458 nm. (d) CLSM images of PLL–PN coacervates at varying SRh concentrations (0–0.06 mM), showing quenching of PN emission and a corresponding increase in SRh emission intensity λ_{ex} = 458 nm. Left panel (green) = PN, Right Panel (orange) = SRh (e) Comparison of percentage energy transfer at 0.03 and 0.06 mM SRh. Scale bar = 20 μm.

between the anionic dyes prevents close proximity and energy coupling (Fig. S16). CLSM imaging further confirms localized FRET-induced sensitization of SRh, even where ensemble fluorimeter measurements yield averaged signals. CLSM revealed increased acceptor emission in regions of donor excitation, confirming localized FRET-induced sensitization (Fig. 2c, d and S17). As FRET is a stochastic, distance-dependent process, the ensemble fluorescence intensity reflects an averaged transfer probability over many donor–acceptor pairs. Therefore, while bulk fluorimetry may underestimate localized events, microscopy effectively resolves FRET-active microdomains. Control experiments excluding the acceptor or altering excitation confirmed negligible direct excitation of the acceptor, validating that observed acceptor emission arises from donor energy transfer rather than spectral crosstalk (Fig. S18).

Conclusions

These results demonstrate that the coacervate microenvironment enables efficient FRET through nanoscale confinement and electrostatic templating of donor–acceptor pairs. The charged, crowded matrix of PLL coacervates modulates dye behaviour by balancing local enrichment and aggregation-induced quenching, thereby tuning the fluorescence and energy-transfer efficiency. Consequently, coacervates function as dynamic soft templates for photonic coupling and nanoscale energy transduction, bridging biological phase separation and functional material design. The mechanistic insights provided here establish design principles for coacervate-based photonic, sensing, and energy-transfer systems in which the optical performance can be precisely tuned *via* electrostatic interactions and phase architecture.

Author contributions

Conceptualization – MK, MKa, and SD; funding acquisition – SD; investigation – MK and MKa; writing – MK, MKa, and SD.

Conflicts of interest

There are no conflicts to declare.

Data availability

The data supporting the findings of this study are included in the article and its Supplementary information (SI), which is accessible through the article see DOI: https://doi.org/10.1039/d5nr04690d.

The raw data are available in a public repository at: https://doi.org/10.5281/zenodo.17536347

 This journal is © The Royal Society of Chemistry 2026

Open Access Article. Published on 11 February 2026. Downloaded on 2/26/2026 3:44:54 AM.
This article is licensed under a Creative Commons Attribution 3.0 Unported Licence.

Acknowledgements

This project was funded by the Deutsche Forschungsgemeinschaft (DFG, German Research Foundation) as part of the Collaborative Research Center "Defects and Defect Engineering in Soft Matter" (SFB 1552), Project No. 465145163. Funding from the DFG is acknowledged: S. D. is a member of the GRK 2516 (Project No. 405552959) and M. K. is the recipient of a doctoral position within the GRK 2516 program. Special thanks to Prof. S. Seiffert for spectroscopy and microscopy facilities.

References

1 L. Leon, G. M. Santiago and E. Spruijt, *Commun. Chem.*, 2024, **7**, 275.
2 S. Patra, B. Sharma and S. J. George, *J. Am. Chem. Soc.*, 2025, **147**, 16027–16037.
3 S. Koppayithodi and N. Singh, *J. Am. Chem. Soc.*, 2025, **147**, 5293–5299.
4 A. Mishra, A. J. Patil and S. Mann, *Chem*, 2025, **11**, 102379.
5 A. Sanchez-Fernandez, I. Insua and J. Montenegro, *Commun. Chem.*, 2024, **7**, 223.
6 A. B. Cook, S. Novosedlik and J. C. M. van Hest, *Acc. Mater. Res.*, 2023, **4**, 287–298.
7 E. R. J. Granda, H. Karoui, X. Brilland, J.-C. Baret and N. Martin, *Chem. – Eur. J.*, 2025, **31**, e202501109.
8 A. Higuchi, A. Som, R. Wakabayashi, M. Goto, N. Kamiya and P. Besenius, *Chem. – Eur. J.*, 2025, **31**, e202404233.
9 L. Su, J. Mosquera, M. F. J. Mabesoone, S. M. C. Schoenmakers, C. Muller, M. E. J. Vleugels, S. Dhiman, S. Wijker, A. R. A. Palmans and E. W. Meijer, *Science*, 2022, **377**, 213–218.
10 H. Duijs, M. Kumar, S. Dhiman and L. Su, *J. Am. Chem. Soc.*, 2024, **146**, 29759–29766.
11 A. Amirsadeghi, R. Parlato, A. Kenbeek, A. R. Gaspar, M. Oggioni, A. Lasorsa, A. Mukherjee, M. Jaber, M. K. Włodarczyk-Biegun, P. C. A. van der Wel, M. Kamperman and G. M. Santiago, *Commun. Chem.*, 2025, **8**, 264.
12 J. Wang, M. Abbas, Y. Huang, J. Wang and Y. Li, *Commun. Chem.*, 2023, **6**, 243.
13 C. Donau, F. Späth, M. Stasi, A. M. Bergmann and J. Boekhoven, *Angew. Chem., Int. Ed.*, 2022, **61**, e202211905.
14 W. Liu, J. Deng, S. Song, S. Sethi and A. Walther, *Commun. Chem.*, 2024, **7**, 100.
15 S. Chowdhuri, S. Das, R. Kushwaha, T. Das, B. K. Das and D. Das, *Chem. – Eur. J.*, 2023, **29**, e202203820.
16 Priyanka, M. Kaur and S. Maiti, *Chem. Commun.*, 2024, **60**, 9101–9104.
17 S. Biswas, M. Haouas, C. Freitas, C. V. Soares, A. Al Mohtar, A. Saad, H. Zhao, G. Mouchaham, C. Livage, F. Carn, N. Menguy, G. Maurin, M. L. Pinto and N. Steunou, *Chem. Mater.*, 2022, **34**, 9760–9774.
18 B. Jing, J. Qiu and Y. Zhu, *Soft Matter*, 2017, **13**, 4881–4889.
19 E. Kluczka, V. Rinaldo, A. Coutable-Pennarun, C. Stines-Chaumeil, J. L. R. Anderson and N. Martin, *ChemCatChem*, 2024, **16**, e202400558.
20 I. B. A. Smokers, B. S. Visser, A. D. Slootbeek, W. T. S. Huck and E. Spruijt, *Acc. Chem. Res.*, 2024, **57**, 1885–1895.
21 Y. Bao and J. Xia, *JACS Au*, 2025, **5**, 5267–5285.
22 M. Kumar, J. N. S. Hanssen and S. Dhiman, *ChemSystemsChem*, 2024, **6**, e202400013.
23 F. P. Cakmak, A. M. Marianelli and C. D. Keating, *Langmuir*, 2021, **37**, 10366–10375.
24 K. P. Sonu, S. Vinikumar, S. Dhiman, S. J. George and M. Eswaramoorthy, *Nanoscale Adv.*, 2019, **1**, 1847–1852.
25 J. Sun, G. M. Santiago, W. Zhou, G. Portale and M. Kamperman, *ACS Sustainable Chem. Eng.*, 2022, **10**, 15968–15977.
26 A. Sarkar, S. Dhiman, A. Chalishazar and S. J. George, *Angew. Chem., Int. Ed.*, 2017, **56**, 13767–13771.
27 C. M. Green, D. Sementa, D. Mathur, J. S. Melinger, P. Deshpande, S. Elbaum-Garfinkle, I. L. Medintz, R. V. Ulijn and S. A. Díaz, *Commun. Chem.*, 2024, **7**, 49.
28 A. J. P. Teunissen, C. Pérez-Medina, A. Meijerink and W. J. M. Mulder, *Chem. Soc. Rev.*, 2018, **47**, 7027–7044.
29 A. J. Amali, S. Singh, N. Rangaraj, D. Patra and R. K. Rana, *Chem. Commun.*, 2011, **48**, 856–858.
30 R. Nandi and N. Amdursky, *Acc. Chem. Res.*, 2022, **55**, 2728–2739.
31 R. Kumar, R. Yadav, M. A. Kolhe, R. S. Bhosale and R. Narayan, *Polymer*, 2018, **136**, 157–165.
32 J. Liu, R. Wang, X. Wang, K. Liang, W. Shi and C. Lu, *J. Mater. Chem. C*, 2023, **11**, 5979–5986.
33 P. Legentil, F. Leroux, R. Mahiou, S. Therias, D. Boyer, F. Reveret, L. Nauton, V. Thery, R. Valleix and G. Chadeyron, *Mater. Adv.*, 2022, **3**, 1200–1211.